Journal of South American Earth Sciences 112 (2021) 103630

Contents lists available at ScienceDirect

Journal of South American Earth Sciences

journal homepage: www.elsevier.com/locate/jsames

Evaluation of deep-water environmental conditions during the latest Maastrichtian-early Danian: Insights from the western south atlantic ocean

Guilherme Krahl [a,b,*], Karlos G.D. Kochhann [a,b], Gerson Fauth [a,b], Alcides N. Sial [c], Luiz Drude de Lacerda [d]

[a] Technological Institute of Paleoceanography and Climate Changes (itt Oceaneon), UNISINOS University, 93022-750, São Leopoldo, Brazil
[b] Geology Graduate Program, UNISINOS University, 93.022-750, São Leopoldo, Brazil
[c] NEG-LABISE, Department of Geology, Federal University of Pernambuco, 50740-530, Recife, Brazil
[d] LABOMAR, Institute of Marine Sciences, Federal University of Ceará, 60165-081, Fortaleza, Brazil

ARTICLE INFO

Keywords:
Volcanism
Mercury (Hg)
Benthic foraminifera
Cretaceous-paleogene
DSDP Site 356

ABSTRACT

The Cretaceous-Paleogene (K-Pg) boundary extinction event affected planktic foraminiferal assemblages worldwide in a dramatic way, but deep sea benthic foraminiferal assemblages were not significantly impacted. However, possible impacts of massive early Danian volcanic eruptions, such as those related to the Deccan Traps, on benthic foraminiferal assemblages are not yet explored. Here we present geochemical and benthic foraminiferal data across the K-Pg boundary and within the earliest Danian interval at Deep Sea Drilling Project (DSDP) Site 356, located on the São Paulo Plateau, western South Atlantic Ocean. Maastrichtian to Danian benthic foraminiferal assemblages are well-preserved and suggest deposition at middle to lower bathyal paleodepths, under an oligotrophic regime with well-oxygenated bottom water conditions. As expected, the K-Pg boundary event did not significantly affect benthic foraminiferal assemblages at Site 356. However, during the early Danian, benthic foraminiferal species richness, heterogeneity, diversity and equitability presented overall opposite trends in relation to the Hg/TOC and Hg/$CaCO_3$ ratios, as well as Hg concentrations, which we consider proxies for intensity of volcanic activity. Our results suggest a possible response of Danian middle to lower bathyal benthic foraminiferal assemblages at Site 356 to changes in bottom water condition possibly associated with massive volcanism eruptions.

1. Introduction

The Cretaceous-Paleocene (K-Pg) boundary, also marking the transition between the Maastrichhtian and the Danian ages, is characterized by one of the largest mass extinctions in Earth's geological history (Gradstein et al., 2012). This event triggered one of the most significant biological crises in the geological record, which is used to define the boundary between the Mesozoic and Cenozoic eras (Molina, 2015). At the boundary level, deep-sea benthic foraminiferal assemblages were not severely affected by the extinction event (e.g., Thomas, 1990; Alegret et al., 2003; Culver, 2003; Alegret and Thomas, 2007), in contrast to patterns described for planktic foraminifera (e.g., Luterbacher and Premilo-Silva, 1962, 1964; Koutsoukos, 1996, 2014; Gallala et al., 2009; Arenillas et al., 2018; Molina, 2015). Minor and temporary compositional changes in benthic foraminiferal communities, reported for several locations worldwide, are mainly interpreted as responses to a collapse in the pelagic food chain, which likely resulted in decreased food availability for benthic organisms (e.g., Alegret et al., 2003; Culver, 2003; Alegret and Thomas, 2007). In fact, several paleoceanographic records also depict a drop in $CaCO_3$ content at the K-Pg transition (Zachos and Arthur, 1986), which was probably related to decreased carbonate production related to the extinction of calcifying organisms (D'Hondt, 2005). Recent studies, however, have shown a heterogeneous post-extinction ocean, with high export productivity in some regions driven by non-calcareous phytoplankton blooms (e.g., Sepúlveda et al., 2012; Hull and Norris, 2011; Alegret et al., 2012) and, less usually, calcareous plankton blooms (Bralower et al., 2020).

The K-Pg mass extinction is most commonly attributed to a meteorite impact at the Chicxulub impact site, Mexico (Schulte et al., 2010), which is mainly evidenced by iridium anomalies (Alvarez et al., 1980), microspherules and quartz grains with shock structures (Smit, 1990) identified in sedimentary records worldwide. An additional factor that

* Corresponding author. Technological Institute of Micropaleontology (itt Fossil), UNISINOS University, 93022-750, São Leopoldo, Brazil.
E-mail address: geounikrahl@gmail.com (G. Krahl).

https://doi.org/10.1016/j.jsames.2021.103630
Received 6 July 2021; Received in revised form 29 October 2021; Accepted 8 November 2021
Available online 19 November 2021

may have contributed to the environmental changes occurred during the Maastrichtian-Danian transition is the eruption of the Deccan Traps Large Igneous Province (LIP), located in present-day India (Courtillot and Renne, 2003). Deccan Traps eruptions lasted for ~700–800 kyr (Schoene et al., 2021), starting earlier and spanning much beyond the actual K-Pg boundary (Hull et al., 2020).

Mercury (Hg) is a potential tracer for volcanic events, because it is usually released by LIP's activity (e.g., Sial et al., 2014, 2016, 2018; Percival et al., 2015; Font et al., 2016) and/or volcanic activity (e.g., Varekamp and Buseck, 1981, 1986). As a result, many studies have observed positive excursions of Hg concentrations and the Hg/TOC (mercury over total organic carbon) ratio in upper Maastrichtian to lower Danian sedimentary successions (Sial et al., 2014, 2016, 2018). Variations of Hg concentrations measured in sedimentary archives that preserved microfossils, and recorded the K-Pg biotic crises, can potentially reveal the impacts of the Deccan Traps volcanism in deep ocean environmental conditions.

Here we aim to assess benthic foraminiferal faunal (compositional) changes across the Maastrichtian-Danian transition in the western South Atlantic Ocean, and to investigate whether they were correlated to Hg enrichment trends. To achieve these goals, we investigate Deep Sea Drilling Project (DSDP) Site 356, located on the São Paulo Plateau, which is characterized by excellent calcium carbonate preservation, and is, therefore, ideal to explore possible links between geochemical proxies and distribution patterns of calcareous microfossils during the late Maastrichtian to early Danian.

2. Material and methods

2.1. Site location and age model

DSDP Site 356 is located on the southwestern São Paulo Plateau (28°17.22′ S, 41°05.28′ W; at 3.175 m water depth) (Fig. 1a). Recovery at Site 356 spans Albian to Recent sediments (Perch-Nielsen et al., 1977), and the section is divided into seven lithological units. Here we focus on the Maastrichtian to lower Paleocene (Danian) interval (415.25–404.26 m below seafloor - mbsf), which is characterized by pelagic carbonate sediments assigned to lithologic Unit 4, described as a nannofossil and nannofossil-foraminifer chalk (Perch-Nielsen et al., 1977). The sediments of the Cretaceous/Paleogene boundary were deposited under oxic conditions and the supply of terrigenous material was cut off during the late Maastrichtian (Perch-Nielsen et al., 1977). Age assignments discussed here are based on planktic foraminiferal biostratigraphy of Kochhann et al. (2014) and Krahl et al. (2017). The age model for the studied interval of Site 356 is based on linear interpolation between the following tie points: First occurrence (FO) of *Pseudoguembelina hariaensis* (67.30 Ma; Gradstein et al., 2012); the K-Pg boundary, identified by an abrupt drop in carbonate content at Site 356 (66.022 Ma; Dinarès-Turell et al., 2014); last occurrence (LO) of *Parvularugoglobigerina eugubina* (65.72 Ma; Gradstein et al., 2012); FO of *Subbotina triloculinoides* (65.25 Ma. Gradstein et al., 2012) (Fig. 1b).

2.2. Benthic foraminiferal assemblages

We analyzed benthic foraminiferal assemblages of 13 samples over the lower Paleocene (Danian) interval at Site 356. Sediment samples

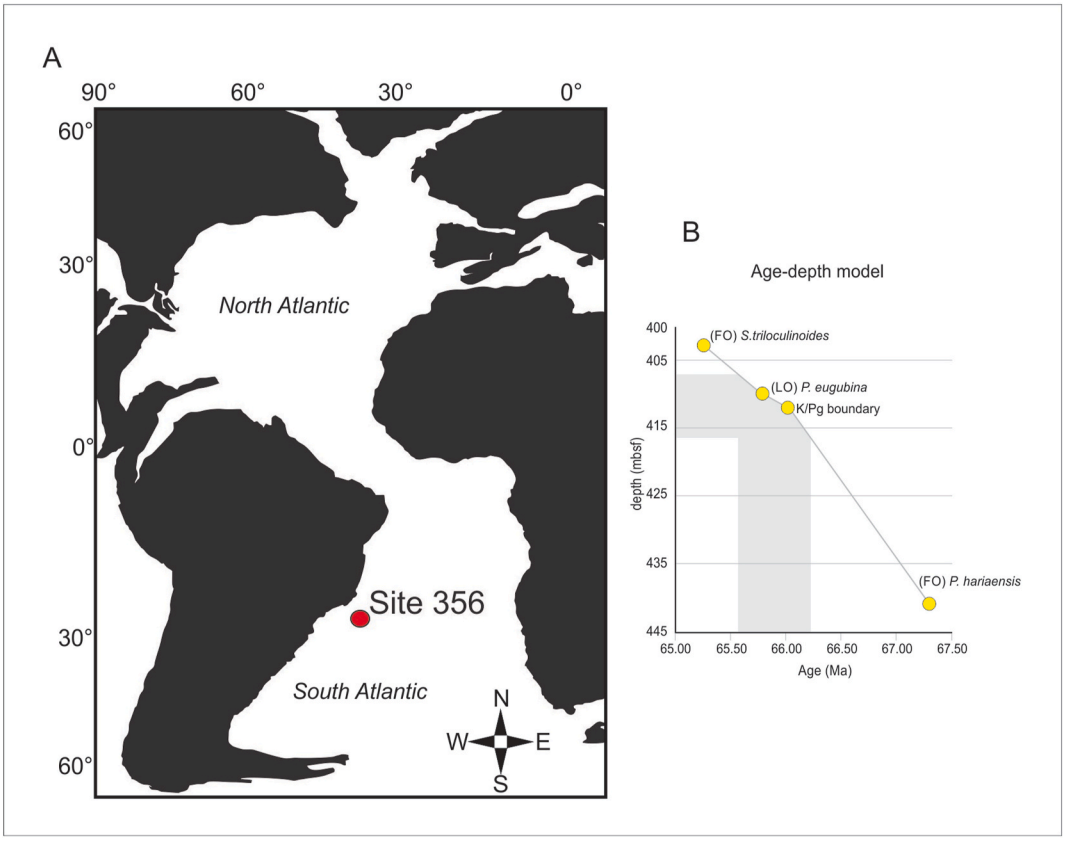

Fig. 1. (A) Paleogeographic reconstruction for the Cretaceous-Paleogene (K-Pg) transition, presenting the reconstructed location of DSDP Site 356 (São Paulo Plateau). Map created with the ODSN paleogeographic reconstruction tool (www.odsn.de/odsn/services/paleomap). (B) Age model for the Maastrichtian-Danian interval of Site 356 based on planktic foraminiferal biostratigraphy (Kochhann et al., 2014; Krahl et al., 2017) and the position of the K-Pg boundary at 66.022 Ma. (Dinarès-Turell et al., 2014). Gray shading represents the studied interval (415.25–404.26 mbsf). Tie points used for the Site 356 are: the FO of *Pseudoguembelina hariaensis* (440.76 mbsf); the K/Pg boundary (410.75 mbsf); the LO of *Parvularugoglobigerina eugubina* (409.25 mbsf); the FO of *Subbotina triloculinoides* (402.77 mbsf).

were washed over 38 μm and 63 μm sieves, after remaining immersed in deionized water for about 48 h. Residues were oven-dried at ~40 °C for ~48 h and about 300 benthic foraminiferal specimens were picked from the >63 μm grain size residues.

Taxonomic analysis was performed under steromicroscope and with a Zeiss EVO MA 15 scanning electron microscope (SEM) at the Technological Institute of Micropaleontology (itt Fossil - UNISINOS University). Generic identifications follow Loeblich and Tappan (1987) and Hayward et al. (2012), while identifications at species level are mainly based on comparisons with studies by Tjalsma and Lohmann (1983), Boltovskoy and Boltovskoy (1989), Boltovskoy and Watanabe (1994), and Alegret and Thomas (2001, 2007). In this work we used the bathymetric subdivisions of Van Morkhoven et al. (1986) and Berggren and Miller (1989): neritic = 0–200 m, upper bathyal = 200–600 m, middle bathyal = 600–1000 m, lower bathyal = 1000–2000 m, and abyssal >2000 m.

We calculated Fisher-α diversity, Shannon (*H'*) heterogeneity, equitability (J), and species richness (S) for each sample, using the software PAST – Paleontological Statistics (Hammer et al., 2001) and considering relative abundances of taxa (e.g., Alegret and Thomas, 2007). R-mode hierarchical cluster analysis was also performed using the software PAST, in order to identify groups of species with similar distribution patterns. Weighted average pair algorithm (UPGMA) and Pearson correlation were used as a similarity coefficient. A smaller dataset, with relative abundances of 26 species (those with relative abundance >2% in at least one sample), was used in the cluster analysis.

2.3. Total organic carbon (TOC) and calcium carbonate ($CaCO_3$) content analyses

Calcium carbonate ($CaCO_3$) and total organic carbon (TOC) contents were measured in 15 samples over the Maastrichtian-lower Paleocene (Danian) interval at Site 356. Sediment samples were oven-dried at 38–60 °C for 48 h. For total carbon (TC) measurements, ~0.26 g of ground and homogenized bulk sediments was measured in a LECO SC-144DR Sulfur and Carbon Analyzer at itt Fossil. TOC content was also measured on an aliquot of ~0.26 g of homogenized bulk sediments, after acidification with hydrochloric acid (HCl 6N, 1:1), followed by washing with distilled water to achieve a neutral pH. $CaCO_3$ content was then calculated based on CT and TOC measurements following the equation of Stax and Stein (1995). Mean standard error based on duplicate samples is ±0.05‰ for TC and TOC.

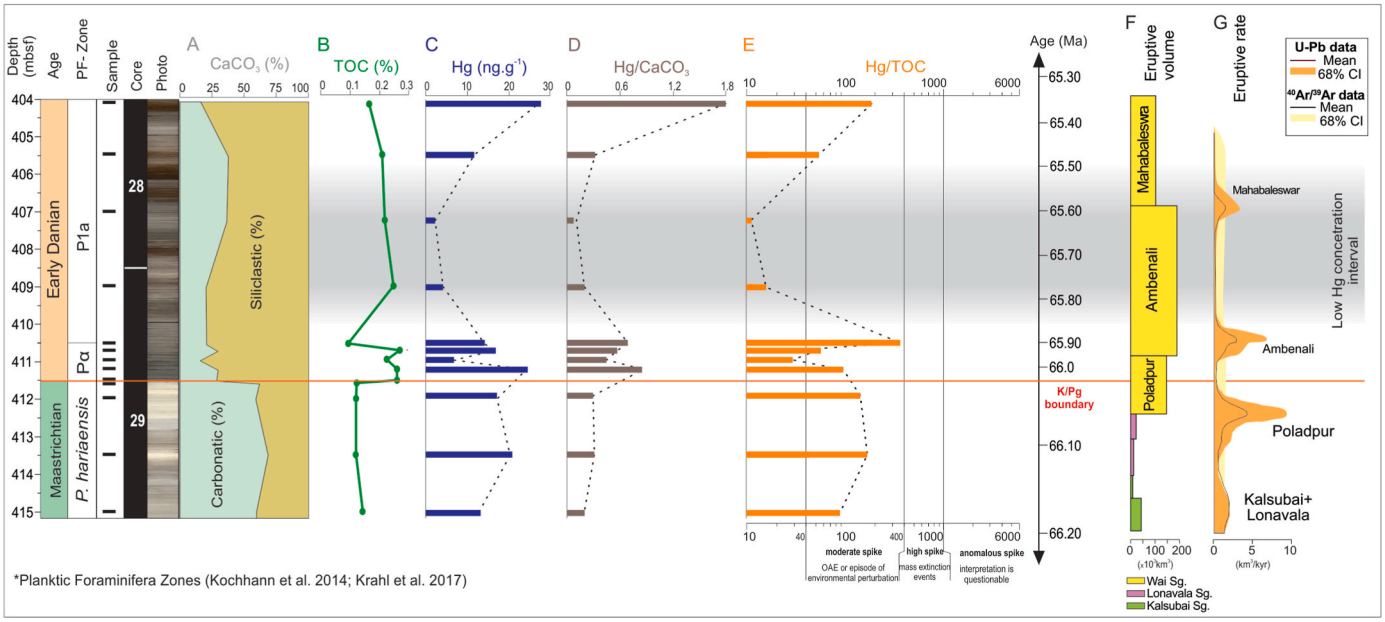

Fig. 2. Geochemical data for the Maastrichtian-Danian interval at DSDP Site 356. (A) carbonate and siliciclastic contents; (B) TOC content; (C) Hg concentrations; (D) Hg/$CaCO_3$ ratio; (E) Hg/TOC ratio; (F) model for Deccan Traps eruption volume (Sprain et al., 2019); (G) model for Deccan Traps eruption rates (Schoene et al., 2019, 2021, 2021). Gray shading marks the interval of low Hg concentrations, Hg/$CaCO_3$ and Hg/TOC ratios. Interpretation of Hg/TOC environmental perturbation levels (in E) according to Charbonnier et al. (2020). Planktic foraminiferal zones follow Kochhann et al. (2014) and Krahl et al. (2017).

Table 1
Geochemical data for the Maastrichtian-Danian interval of DSDP Site 356.

Sample	Depht (mbsf)	Age (Ma)	TOC (wt%)	CaCO3 (%)	Hg (ng.g-1)	Hg/CaCO3	Hg/TOC	Age
356-28-4 (73–75)	404.26	65.358	0.161	15.96	29.2	1.830	181.220	Danian
356-28-5 (73–75)	405.73	65.465	0.209	37.66	11.9	0.316	56.908	
356-28-6 (76–77.5)	407.26	65.576	0.218	36.27	2.3	0.063	10.532	
356-29-1 (75–78)	409.25	65.720	0.269	20.08	4.2	0.209	15.627	
356-29-2 (77–78.5)	410.77	65.899	0.041	20.59	14.6	0.709	359.677	
356-29-2 (95–97)	410.95	65.920	0.293	29.27	17	0.581	57.941	
356-29-2 (120–123)	411.20	65.949	0.225	15.48	6.9	0.446	30.605	
356-29-2 (145–148)	411.45	65.979	0.259	29.46	24.9	0.845	96.128	
356-29-3 (25–27)	411.75	66.014	0.259	28.35	no data	no data	no data	
356-29-3 (32–34)	411.82	66.022	0.122	61.78				Maastrichtian
356-29-3 (75–78)	412.25	66.041	0.120	58.85	17.6	0.299	146.667	
356-29-4 (74–76)	413.74	66.107	0.120	68.42	20.9	0.305	174.065	
356-29-5 (75–77)	415.25	66.173	0.143	59.02	13.1	0.222	91.449	

Table 2
Benthic foraminiferal relative abundances, species richness, heterogeneity, diversity, equitability at DSDP Site 356. Taxa are grouped by clusters to A, B and C.

Age	*Depth(mbsf)*	*Age(Ma)*	*Fragments*	*Indet.*	*Lagenasulcata*	*Hauerinidaespp.*	*Chrysalogoniumequisetiformis*(Schwager, 1866)	*Praebulimineareussi*(Morrow, 1934)	*Astaculussp.*	*Buliminatrinitatensis*Cushman and Jarvis, 1928	*Aragoniavelascoensis*(Cushman, 1925)	*Quadrimorphinaallomorphinoides*(Reuss, 1860)	*Laevidentalinasp.2*	*Oridorsalisumbonatus*(Reuss, 1851)	*Stensioeinabeccariiformis*(White, 1928)	*Bulimina simplex*Terquem, 1882	*Cibicidoideshyphalus*(Fischer, 1969)	*Anomalinoidessp.*	*Paralabaminalunata*(Brotzen, 1948)	*Paralabaminahillebrandti*(Fisher, 1969)	*Nuttallidestruempyi*(Nuttall, 1930)	*Pullenia jarvis*iCushman, 1936	*Bolivinoidessp.*	*Lenticulinaconvergens*(Bornemann, 1855)	*Allomorphinaconica*Cushman and Todd, 1949	*Strictocostellahispidula*(Cushman, 1939)	*Bulimine llabeaumonti*Cushman and Renz, 1946	*Buliminamidwayensis*(Cushman and Parker, 1936)	*Pyramidinarudita*(Cushman and Parker, 1935)	*Laevidentalinasp.1*	*Gyroidinoidessoldanii*(d'Orbigny, 1826)
	404.26	65.358	26	0	0	0	3	0	0	9	0	2	6	16	9	7	27	17	29	4	29	0	6	3	5	6	3	11	6	3	10
	405.73	65.465	26	1	0	3	4	0	0	0	0	0	5	9	9	4	25	18	19	6	16	1	13	5	2	21	5	7	2	9	9
	407.26	65.576	28	1	2	2	3	0	0	3	0	0	4	10	9	1	32	23	24	2	17	6	18	5	2	12	4	6	4	3	11
	409.25	65.720	29	0	2	1	0	0	0	0	0	0	2	9	8	0	38	31	37	6	12	5	26	3	1	12	3	9	7	4	25
	410.77	65.899	28	0	0	0	0	0	0	3	1	6	3	22	0	1	6	46	42	3	22	7	12	4	5	2	4	8	11	4	14
	410.95	65.920	32	0	4	2	3	6	8	5	2	2	7	14	6	0	9	39	44	1	17	4	1	2	6	7	6	1	4	8	12
	411.20	65.949	28	0	5	1	0	8	2	8	6	3	3	28	2	0	4	28	42	5	22	8	6	2	7	4	7	4	5	9	12
	411.45	65.979	29	2	0	1	3	3	3	3	2	1	5	15	1	2	18	25	36	2	23	13	10	2	0	2	5	8	9	1	13
	411.75	66.014	12	1	0	1	2	7	1	6	1	1	2	16	13	5	66	31	24	3	13	3	4	3	1	6	10	5	2	2	18
	411.82	66.022	19	2	2	3	2	3	4	4	1	1	0	0	22	5	78	16	6	5	31	10	3	3	1	7	3	6	3	1	21
	412.25	66.041	22	1	1	3	1	7	2	4	0	2	0	13	15	4	91	15	13	11	29	10	2	1	1	2	3	4	10	0	12
	413.14	66.107	24	2	1	2	1	13	3	5	1	1	2	20	18	2	49	12	23	11	37	7	1	1	2	3	4	5	10	6	16
	415.25	66.173	29	1	2	1	3	9	1	3	1	4	4	17	21	1	56	18	14	11	49	6	2	0	0	4	2	6	8	6	9

*Pleurostomelliacuta*Hantken, 1875	*Gaudryinapyramidata*(Cushman, 1926)	*Marssonellasp.*	*Pyrulinaspp.*	*Valvulinaspinosas*Cushman, 1927	*Fissurinaspp.*	*Pulleniabulloidesd'*Orbigny(1846)	*Marssonellasp.*1	*Oxangulariavelascoensis*(Cushman, 1925)	*Cibicidoides?sp.*	*Saracenariasp.*	*Lagenaspp.*	*Laevidentalinasp.*3	*Anomalinoidessp.*1	*Coryphostomaincrassata*(Reuss, 1851)	*Bolivinopsiscubensis*(CushmanandBermúdez, 1937)	*Lenticulinasp.*	*Ellipsoglandulinasp.*	*Hemirobuliminasp.*1	*Glomospirasp.*	*Planulinasp.*	*Stilostomellasp.*2	*Nodosariasp.*1	*Buliminaaff.kugleri*(CushmanandRenz, 1942)	*Coryphostomasp.*	*Bolivinoidesdecoratus*(Jonesetal., 2019)	*Richness*(*species*)	*Shannon – Wiener*	*Equitability*	*Fisher*	*SubclusterA*	*SubclusterB*	*SubclusterC*
13	7	1	12	2	6	0	3	1	0	0	5	0	0	4	0	3	1	0	0	0	2	0	0	3	0	35	3.189	0.8968	10.65	14.85	35.31	28.71
14	3	1	12	4	3	0	7	2	2	0	9	0	1	5	3	4	1	0	0	0	6	1	2	2	0	41	3.361	0.9051	13.34	21.26	29.24	22.26
14	2	2	7	6	4	1	6	0	0	2	4	2	0	0	2	3	3	1	0	1	5	1	0	1	0	43	3.296	0.8764	14.4	16.28	29.90	27.57
7	1	0	6	4	6	2	6	0	0	2	1	0	0	0	5	2	1	1	0	0	0	0	1	1	1	35	2.989	0.8340	10.86	17.35	30.91	30.60
16	0	0	13	0	6	4	4	0	0	0	2	0	0	0	0	0	0	1	0	0	3	1	0	0	0	30	2.888	0.8491	8.563	9.54	51.32	20.72
10	1	1	9	2	3	0	2	0	1	2	0	0	0	1	0	2	0	0	0	0	0	0	0	0	0	37	3.046	0.8436	11.91	3.99	50.17	22.92
12	1	0	8	5	4	0	7	0	0	0	0	0	0	0	0	0	1	2	0	0	1	0	0	0	0	34	3.082	0.8741	10.26	7.33	51.67	21.33
12	1	0	1	1	2	0	0	0	0	3	0	0	2	0	1	3	1	3	1	17	0	0	0	0	0	39	3.090	0.8434	12.81	8.17	35.29	30.07
14	0	0	5	0	2	0	4	0	0	1	0	2	1	1	1	4	1	2	0	0	0	0	0	0	0	39	2.923	0.7980	12.22	7.97	37.21	41.86
7	4	0	2	1	3	2	0	1	1	1	1	0	0	0	0	0	0	0	0	0	0	0	0	0	0	37	2.747	0.7607	11.68	8.64	14.28	59.14
10	1	1	0	0	1	0	0	0	1	0	0	0	0	0	0	0	0	0	0	0	0	0	0	0	0	33	2.571	0.7486	9.025	3.97	20.37	59.29
6	1	0	2	0	4	1	6	1	0	0	0	0	0	0	0	0	0	0	0	0	0	0	0	0	0	34	2.931	0.8245	10.57	5.77	26.60	50.27
5	4	1	2	2	0	0	0	0	0	0	0	0	0	0	0	0	0	0	0	0	0	0	0	0	0	32	2.803	0.8089	9.352	6.34	22.02	53.37

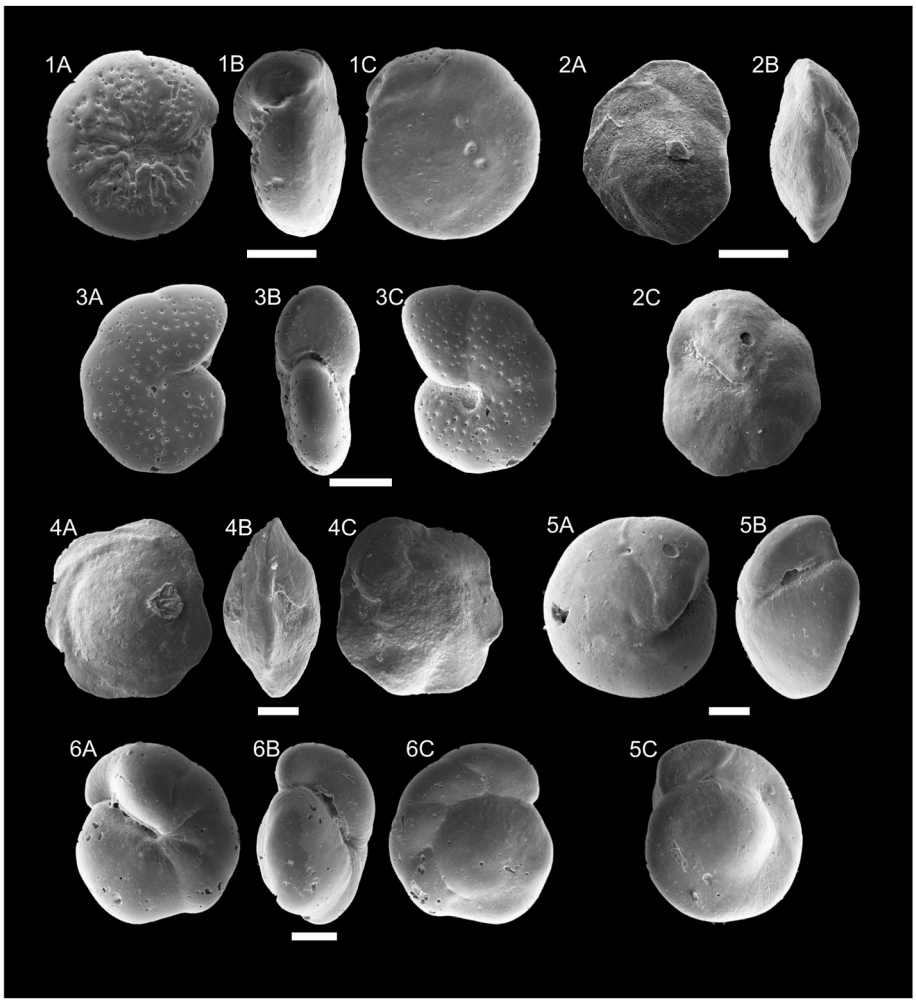

Fig. 3. Representative benthic foraminiferal species recovered from the Cretaceous-Paleogene interval at DSDP Site 356. 1A-C) *Stensioeina beccariiformis* (405.73 mbsf); 2A-C) *Paralabamina lunata* (411.20 mbsf); 3A-C) *Anomalinoides* sp. (404.26 mbsf); 4A-C) *Nuttallides truempyi* (411.82 mbsf); 5A-C) *Oridorsalis umbonatos* (411.20 mbsf); 6A-C) *Gyroidinoides soldanii* (409.25 mbsf). Scale bars represent 100 μm.

2.4. Mercury (Hg) analysis

Mercury (Hg) concentrations were measured on 13 samples (Maastrichtian-lower Danian) from Site 356 at the LABOMAR Laboratory of the Federal University of Ceará, following the procedure described by Sial et al. (2014). For each sample, ~0.9 g of homogenized sediments was oven-dried at 60 °C prior to digestion in a hydrochloric (HCl) and hydrofluoric (HF) acids solution, and heated up to 70 °C for 1 h in an athermic-kinetic reactor. Sample vials were all cleaned with an Extran solution (10% v/v), immersed in an HCl solution (10% v/v) for two extra days and rinsed with Milli-Q water. Hg^{2+} was reduced with $SnCl_2$ and measured with a Cold Vapor Atomic Fluorescence Spectrometer (Millennium Merlin PSA). All samples were measured as duplicates, presenting reproducibility better than 9.5%, and the reference material NIST 2702 was measured for accuracy control.

3. Results

3.1. Geochemical data

Carbonate content was high (>60.0%) in the Maastrichtian, and dropped abruptly at the K-Pg boundary, oscillating between 15.5 and 37.7% in the Danian (Fig. 2A; Table 1). TOC values, on the other hand, remained low throughout the studied interval (Fig. 2B; Table 1). During the Maastrichtian, TOC was ~0.1%, increased above 0.2% at the K-Pg boundary and within the first meter of the Danian section, and fluctuated between 0.0 and 0.3% during the remaining of the Danian.

Mercury concentrations during the Maastrichtian varied between 8.3 and 20.9 ng/g, while the Danian interval of Site 356 displayed the highest amplitude variability, ranging from 2.3 to 29.2 ng/g (Fig. 2C; Table 1). The Hg/TOC ratio displays significant variability in the studied interval (Fig. 2E; Table 1). In the Maastrichtian, Hg/TOC values oscillated between 78.81 and 174.06, and in the Danian between 10.53 and 359.67. The Hg/TOC ratio also peaked in the first centimeters above de K-Pg boundary and at 65.358 Ma (404.26 mbsf). In this work, we also applied the ratio between $Hg/CaCO_3$, since different values of carbonate content were observed. The $Hg/CaCO_3$ ratio was low in the Maastrichtian, and the highest increases in $Hg/CaCO_3$ also occurred in the first centimeters above the K-Pg boundary and at 65.358 Ma (404.26 mbsf), within the Danian (Fig. 2D; Table 1). Both $Hg/CaCO_3$ and Hg/TOC present low values between 407.26 mbsf and 409.25 mbsf (P1a biozone), from ~65.57 to 65.72 Ma (Fig. 2; Table 1). Even though low $CaCO_3$ content following the K-Pg boundary may have influenced trends in the $Hg/CaCO_3$ ratio, it is remarkable that $Hg/CaCO_3$ and Hg/TOC present overall comparable trends throughout the studied interval at Site 356.

3.2. Benthic foraminiferal assemblages

Benthic foraminiferal assemblages at Site 356 are well-preserved and

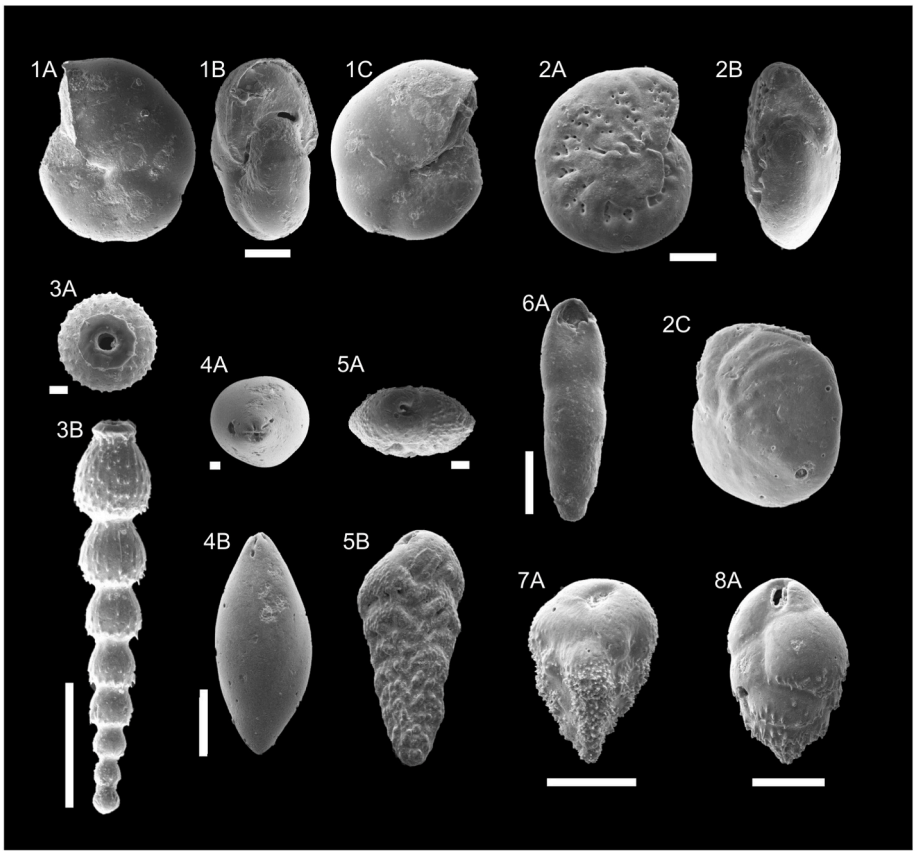

Fig. 4. Representative benthic foraminiferal species recovered from the Cretaceous-Paleogene interval at DSDP Site 356. 1A-C) *Pullenia jarvisi* (411.45 mbsf); 2A-C) *Cibicidoides hyphalus* (407.26 mbsf); 3A-B) *Strictocostella hispidula* (410.95 mbsf); 4A-B) *Pyrulina* spp. (405.73 mbsf); 5A-B) *Bolivinoides* sp. (409.25 mbsf); 6A) *Pleurostomella acuta* (411.75 mbsf); 7A) *Pyramidina rudita* (410.77 mbsf); 8A) *Bulimina midwayensis* (411.45 mbsf). Scale bars represent 100 μm.

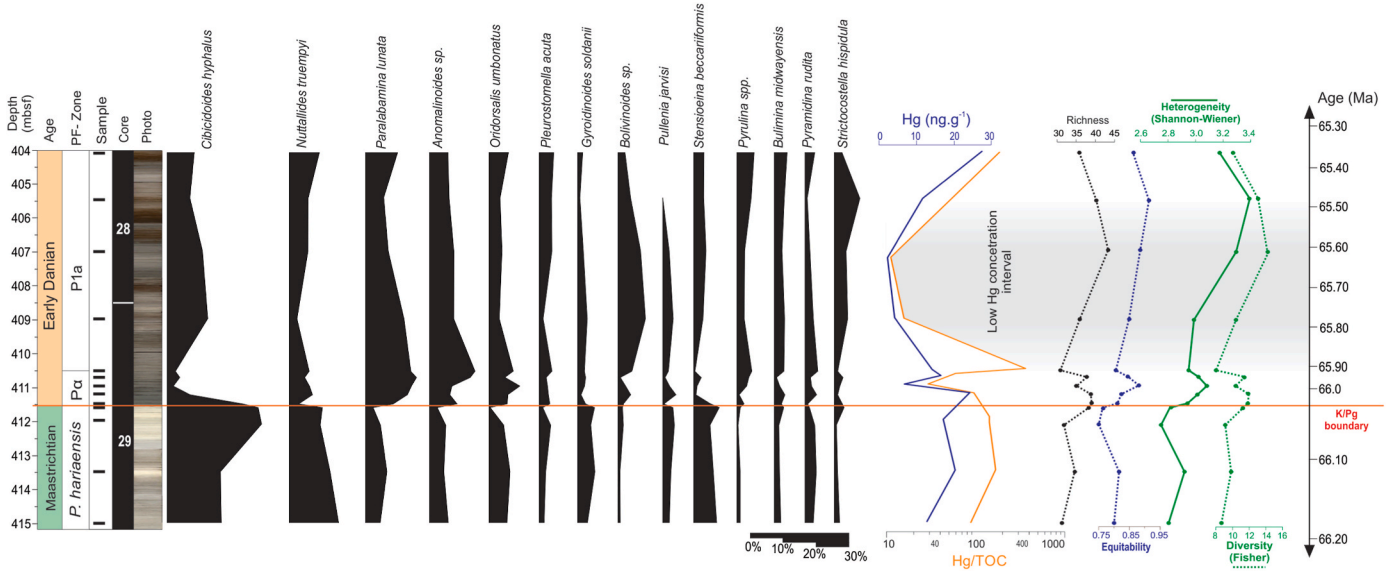

Fig. 5. Benthic foraminiferal distributions over the studied interval at DSDP Site 356. We present relative abundances of the most representative benthic foraminiferal species (with >2% relative abundances), species richness, equitability, Shannon-Weaver index (heterogeneity) index, and Fisher-a index (diversity). Gray shading marks the stratigraphic interval of low Hg concentrations and Hg/TOC ratios (also shown here).

we identified 55 benthic foraminiferal species over the studied interval (Table 2). Overall, calcareous forms dominated assemblages, reaching 96.0–98.7% of total benthic foraminiferal counts (Table 2). Species with relative abundances higher than 2% at Site 356 are presented in Figs. 3 and 4. Assemblages were dominated by *Cibicidoides hyphalus* (12.97%), *Paralabamina lunata* (9.12%), *Anomalinoides* sp. (8.29%), *Nuttallides truempyi* (8.22%), *Oridorsalis umbonatus* (4.84%) and *Gyroidinoides soldanii* (4.67%) (Fig. 5). Together, these species make 48.11% of the total

Table 3
Benthic foraminifera specimes identified at DSDP Site 356, grouped into paleobatimetry preference.

Especime	Bathymetric common distribition
Cibicidoides hyphalus	Lower (a, b) at middle bathyal (c)
Nuttallides truempyi	Middle-lower bathyal and abyssal (a, e, b, f); Bathyal and abyssal (d)
Paralabamina lunata	Bathial to abyssal (c)
Oridorsalis umbonatus	Deep Bathyal (g); Wide wide bathymetric distribution(b)
Pleurostomella acuta	Bathyal (h) to lower bathyal (i)
Gyroidinoides soldanii	Bathyal (h) to upper bathyal (i)
Pullenia jarvisi	Bathyal (h)
Stensioenia beccariformis	Bathyal–abyssal (d); Lower bathyal (b, f); Bathyal (e) and Abyssal (e, f); Bathyal to abyssal (c)
Bulimina midwayensis	Bathial to abyssal (b)
Pyramidina rudita	Middle bathyal (c)
Strictoscostella hispidula	Bathyal (h)

(a) Van Morkhoven et al. (1986); (b) Tjalsma and Lohmann (1983); (c) Widmark and Speijer (1997); (d) Berggren and Aubert (1975); (e) Speijer (1994); (f) Widmark (2000); (g) Alegret and Thomas (2004); (h) Boltovskoy and Watanabe (1994); (i) Culver (1988).

benthic foraminiferal counts and suggest deposition at middle to lower bathyal paleodepths (e.g., Tjalsma and Lohmann, 1983). We also present paleobathymetric preferences for the most representative benthic foraminifer species in Table 3.

Richness, defined as the number of species per sample, varied from 30 to 43 over the studied interval at Site 356. The highest richness value was recognized within the Danian, at 407.26 mbsf (Fig. 5). The equitability index varied between 0.7 (412.25 mbsf) and 0.9 (407.26 mbsf) (Fig. 5). Values closer to 1 (at 405.26 and 407.26 mbsf) indicate a more even distribution of abundances among the taxa of a given assemblage. The Shannon-Wienner and Fisher diversity indexes exhibit overall similar trends (Fig. 5). The Shannon-Wienner index oscillated between 2.6 (412.25 mbsf) and 3.4 (405.73 mbsf), whereas the Fisher index varied between 8.6 (410.77 mbsf) and 14.4 (407.26 mbsf). As a general feature, all diversity indexes show high values for the Danian interval (P1a zone; Fig. 5).

3.2.1. Cluster analysis

Cluster analysis of the benthic foraminiferal faunal data allowed us to identify three main clusters in R mode (Fig. 6). Cluster A includes species that were more abundant in the Danian, after ~65.72 Ma. (P1a zone; Fig. 7). The most representative species in cluster A are *Bolivinoides* sp. and *Strictocostella hispidula*. Similarly, cluster B includes species that were more abundant in the Danian, but more specifically between the K-Pg boundary and ~65.72 Ma. (Pα and lower P1a zones; Fig. 7). The most representative species of cluster B are *Paralabamina lunata, Oridorsalis umbonatus*, *Anomalinoides* sp. and *Pleurostomella acuta*. Cluster C groups species that were more abundant in the Maastrichtian, between ~66.17 Ma (base of the studied interval) and the K-Pg boundary (Fig. 7). For cluster C, the most representative species are *Cibicidoides hyphalus*, *Nuttallides truempyi* and *Stensioeina beccariiformis*.

4. Discussions

4.1. Reliability and significance of the Hg-based proxies

Trends in $CaCO_3$ and TOC contents at Site 356 are similar to those observed in other K-Pg sections, with abrupt drops in $CaCO_3$ content and slight increases in TOC at the transition (e.g., D'Hondt, 2005). TOC remains low throughout the studied interval of Site 356, suggesting that

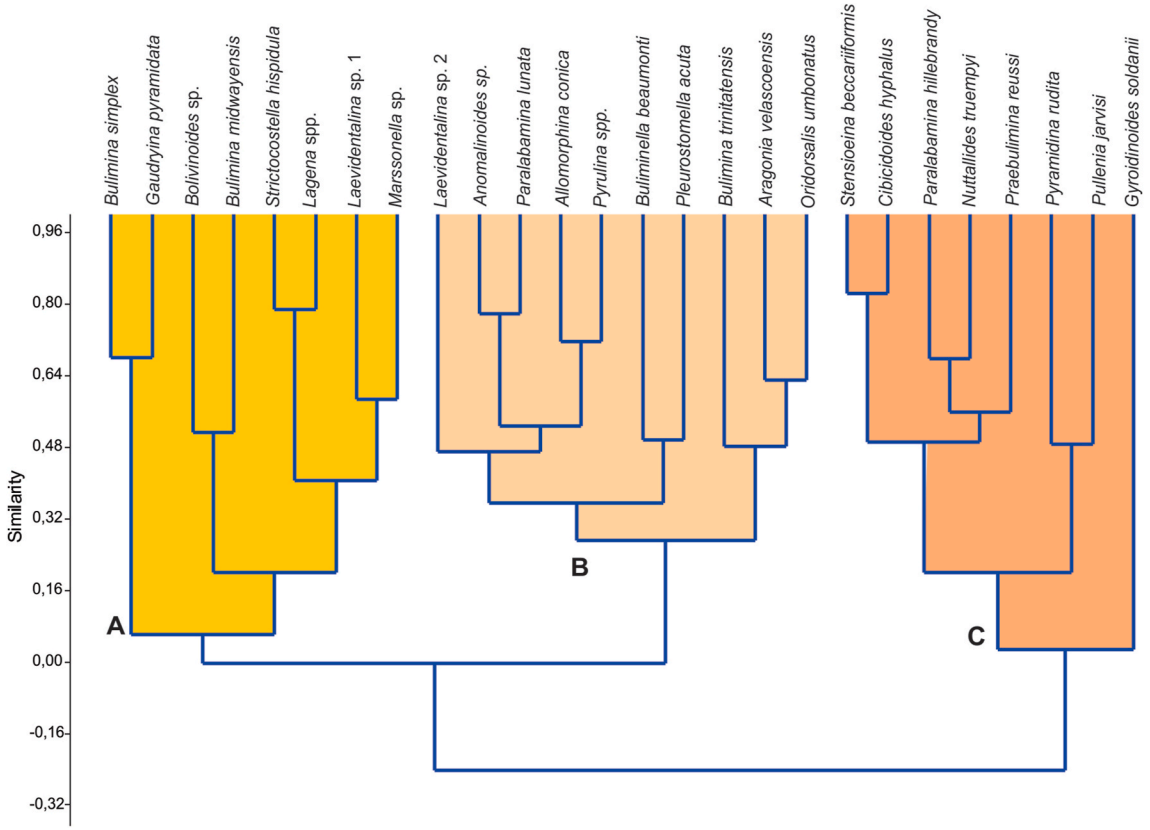

Fig. 6. R-mode hierarchical cluster analysis of benthic foraminiferal relative abundances across the Maastrichtian-Danian transition at DSDP Site 356, with identifications of clusters A-C.

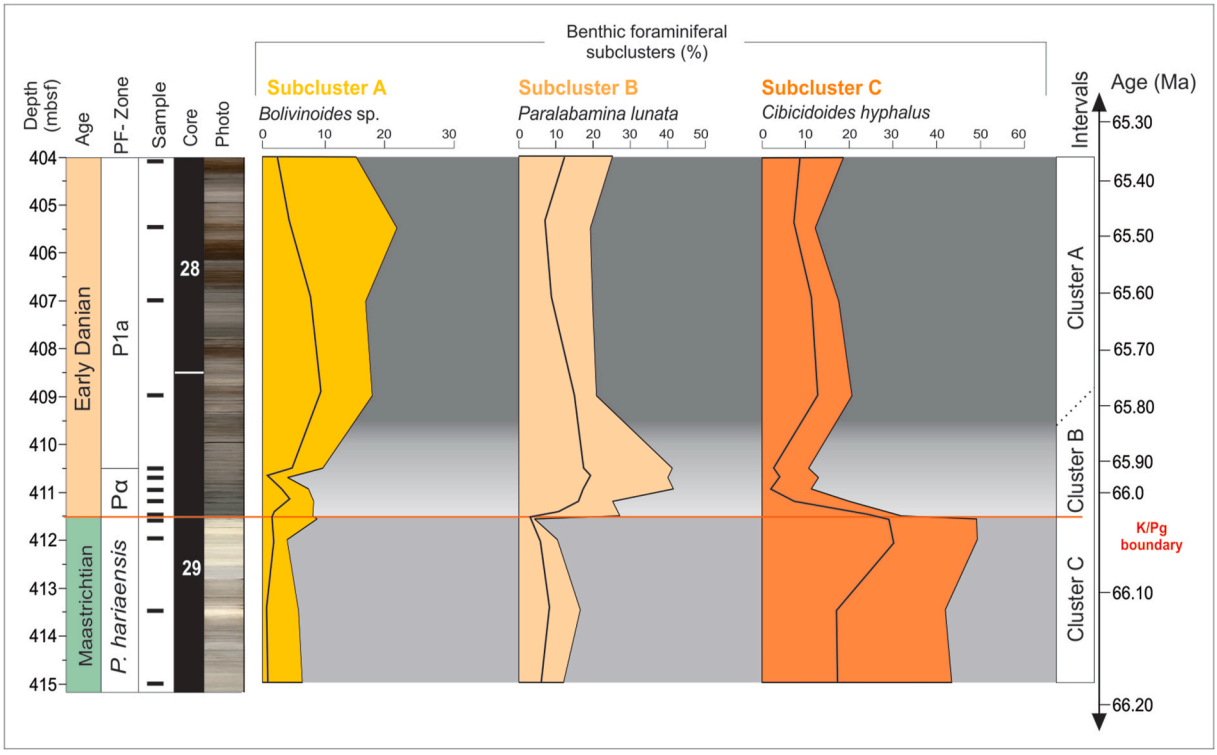

Fig. 7. Relative abundances of clusters A (yellow), B (beige) and C (orange) over the Maastrichtian-Danian transition at Site 356, including the relative abundances of their most representative species (black lines at the center of each area plot). The most abundant species are: *Bolivinoides* sp. for cluster A, *Paralabamina lunata* for cluster B, and *Cibicidoides hyphalus* for cluster C.

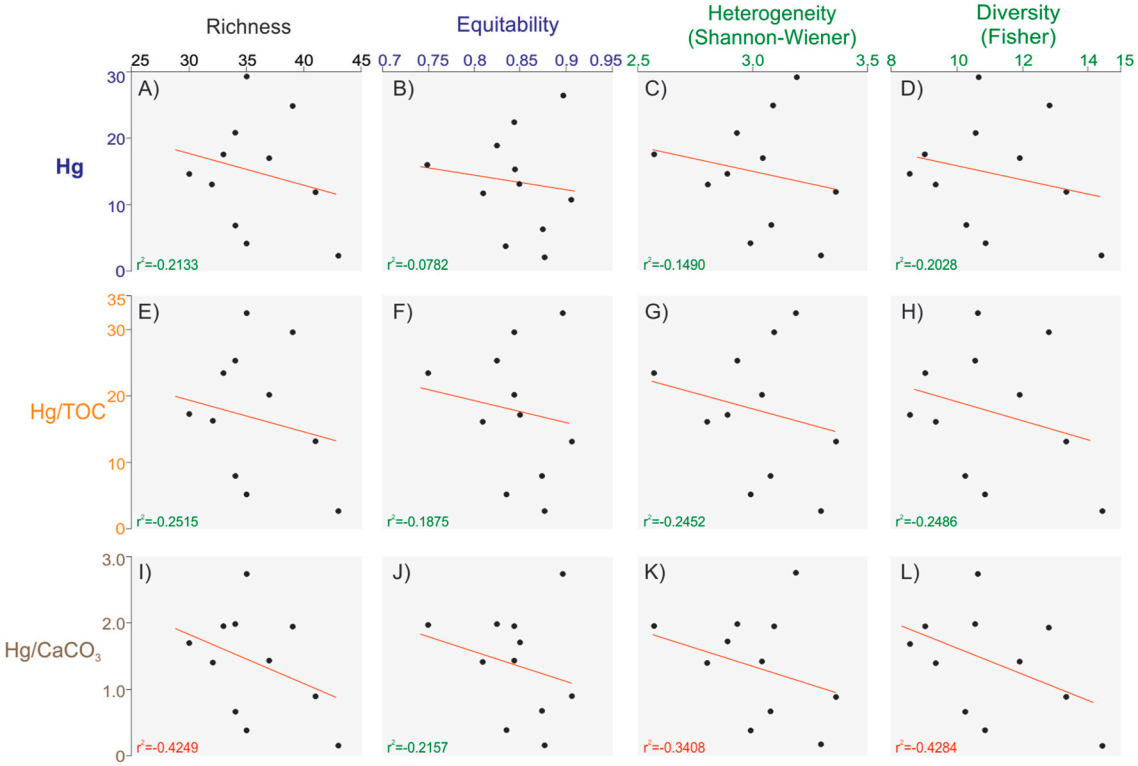

Fig. 8. Cross-plots of geochemical proxies (Hg concentrations, Hg/TOC and Hg/$CaCO_3$) and diversity indexes (Richness, Equitability, Shannon-Wiener diversity and Fisher diversity) at Site 356. (A) Hg vs Richness. (B) Hg vs Equitability. (C) Hg vs Shannon-Wiener diversity. (D) Hg vs Fisher diversity. (E) Hg/TOC vs Richness. (F) Hg/TOC vs Equitability. (G) Hg/TOC vs Shannon-Wiener diversity. (H) Hg/TOC vs Fisher diversity. (I) Hg/$CaCO_3$ vs Richness. (J) Hg/$CaCO_3$ vs Equitability. (K) Hg/$CaCO_3$ vs Shannon-Wiener diversity. (L) Hg/$CaCO_3$ vs Fisher diversity. All r^2 values < -0.3 are shown in green.

the Hg/TOC ratio is not biased by variations in TOC content (Sial et al., 2016). However, Hg/TOC values could be biased for samples with TOC <0.2% (Grasby et al., 2016), which is the case for the Maastrichtian interval of Site 356 (Fig. 2), and/or post depositional alteration of the organic matter (Charbonnier et al., 2020). We consider it unlikely that these low TOC values biased Hg/TOC ratios, since the calculated values for the ratio show only small amplitude variability in the Maastrichtian. For the whole Maastrichtian-Danian interval of Site 356, Hg/TOC presents a strong positive correlation with Hg concentrations (Fig. 2) and values are within the expected range of unbiased Hg/TOC ratios of Charbonnier et al. (2020) (Fig. 2). Furthermore, the Hg/TOC and $Hg/CaCO_3$ ratios show overall similar trend in the Maastrichtian and Danian (Fig. 2D and E), suggesting that Hg-based proxies indeed recorded an environmental signal at Site 356.

We are cautious, however, with interpreting high-resolution Hg/TOC spikes for the Maastrichtian-Danian interval (e.g., Sial et al., 2014, 2016 e 2018), due to the low TOC values mainly within the Maastrichtian. At the K-Pg transition, we can confidently interpret high Hg/TOC values within the uppermost Maastrichtian and lowermost Danian as indicative of a paleoenvironmental disturbance, with Hg/TOC between 40 and 400 (e.g., Charbonnier et al., 2020). These high values of Hg/TOC, and also $Hg/CaCO_3$ and Hg concentrations (Fig. 2), close to the K/Pg boundary are potentially correlated with pulses of the Deccan Traps volcanism in India (e.g., Sprain et al., 2019; Schoene et al., 2019, 2021). Upward in the Site 356 section, the lowest Hg concentrations, and Hg/TOC and $Hg/CaCO_3$ ratios, occurred within the Danian, between ~65.72 and 65. 57 Ma (P1a zone; Fig. 2), suggesting a link with reduced volcanic activity and environmental stability between the Deccan Trap Ambenali and Mahabeleswar formations (pulses).

Our age estimates for this interval with low Hg/TOC ratios at Site 356 (~65.72–65. 57 Ma) agree well with the gap between the main phases of the Deccan Trap volcanic pulses reported by Schoene et al. (2019, 2021) (Fig. 2). However, between the depths of 404.26 (~65.358 Ma) and 407.73 mbsf (~65.465 Ma), Site 356 records increased Hg concentrations (and Hg/TOC and Hg/CaCO3) that do not correlate in age with the Mahabeleswar Formation (pulse; Schoene et al., 2021). This difference may be related to (i) variation in the sedimentation rates at Site 356 through the P1a biozone, (ii) diachronism of the planktic foraminiferal markers used as age-depth tie point in our age model, and/or (iii) differences in the methods used to constrain the Deccan Traps age models. Regarding the latter, our Hg proxy records seem to better agree with the eruption rates of Schoene et al. (2019, 2021), who used U–Pb dating, than with the eruption volume estimates of Sprain et al. (2019), based on Ar^{40}/Ar^{39} dating (Fig. 2). Nevertheless, establishing direct links between Deccan Traps pulses and deep-ocean Hg anomalies requires additional high-resolution studies with well-constrained chronologies.

4.2. Impacts on benthic foraminiferal assemblages

The species *Cibicidoides hyphalus*, *Nuttallides truempyi*, *Paralabamina lunata* and *Anomalinoides* sp. were abundant in the Maastrichtian-Danian interval at Site 356. Therefore, we can suggest that bottom waters were well-oxygenated, probably related to an oligotrophic regime (e.g., Schönfeld and Burnett, 1991; Widmark and Speijer, 1997; Alegret and Thomas, 2007). This inference is also supported by low TOC concentrations. Furthermore, as pointed out by Alegret and Thomas (2013), increased relative abundances of heavily calcified forms, such as *C. hyphalus* and *N. truempyi*, may reflect the occurrence of deep waters supersaturated in carbonate ion, mainly for the interval before the K-Pg extinction event at Site 356 (chron C30r to the K-Pg boundary). These heavily calcified forms were also grouped in cluster C (Figs. 6 and 7), which presents higher relative abundances within the Maastrichtian.

The extinction event at the K-Pg boundary affected several fossil groups, among them planktic foraminifera (e.g., Koutsoukos, 1996, 2014; Gallala et al., 2009; Arenillas et al., 2018). This planktic foraminiferal extinction was also recognized at Site 356 (Krahl et al., 2017). However, benthic foraminiferal assemblages at Site 356 do not record a significant evolutionary turnover at the K-Pg transition. This pattern is in accordance with those described elsewhere, for instance, on the Walvis Ridge (Ocean Drilling Program – ODP Hole 1262C; Alegret and Thomas, 2007), Gulf of Mexico (Alegret et al., 2001), Maud Rise (ODP Site 689–690; Culver, 2003), Broken Ridge (ODP Site 752; Culver, 2003), Hess Rise (DSDP Site 465; Widmark and Malmgren, 1992) and at Coldorso Section (Italy; Coccioni and Savelli, 1983) This observation supports the notion that the environmental effects of the K-Pg boundary event were mostly restricted to shallow waters, as suggest by Culver (2003).

We also observed increased relative abundances of *Stensioeina beccariiformis* and *Cibicidoides hyphalus* (>25%) during the latest Maastrichtian, similar to the pattern described by Alegret and Thomas (2007) for Site 1262, which is geographically close to the location of Site 356. However, at Site 356 diversity increased immediately after the K-Pg, whereas on the Walvis Ridge (Site 1262) diversity indexes dropped. Distinct recovery patterns for post K-Pg paleoproductivity proxy records were also described for the western and eastern South Atlantic Ocean by Hull and Norris (2011).

For the studied interval at Site 356, biostatistical parameters show similar trends. We observed smooth variations in richness, diversity and equitability within the Maastrichtian to Danian interval (Fig. 5). Between ~65.72 and 65.57 Ma (P1a zone), the lowest Hg values (for concentrations and ratios) occurred. This interval, also records slight increases of diversity indexes (Fig. 5). For instance, all diversity indexes show slight negative correlation with Hg concentrations, Hg/TOC and $Hg/CaCO_3$, with the most significative correlations reached r^2 ~0.4 (Fig. 8).

In modern continental and marine aquatic environments, Hg is considered one of the most threatening trace metal pollutants for living organisms (Jiang et al., 2006; Driscoll et al., 2013; Sizmur et al., 2018). Furthermore, Hg is bioaccumulated in aquatic environments as the trophic level increases (Gebka et al., 2018). The effects of water Hg concentrations on modern benthic foraminiferal assemblages from coastal environments are widely reported in the literature (e.g., Frontalini et al., 2018). Drops in diversity, coupled to high Hg concentrations, were reported by Frontalini et al. (2009) and Caruso et al. (2011). In the geological record, however, we consider it unlikely that deep-ocean Hg concentration reached levels compared to those of modern coastal environments.

In addition to an increase in Hg emissions, Deccan Traps volcanism likely increased emissions of carbon dioxide (CO_2) and acids (e.g., HCl; Self et al., 2008). However, the excellent preservation of benthic foraminiferal assemblages at Site 356 (e.g., Boersma, 1977; Kochhann et al., 2014; Krahl et al., 2017), does not support increased deep-ocean ocean acidification associated with the event. Instead, low $CaCO_3$ content in the Danian section of Site 356 suggests a possible role for decreased accumulation of calcareous primary producers in controlling early Danian foraminifera occurrences. This processes could potentially affect food availability for deep-ocean benthic foraminiferal assemblages.

5. Conclusions

Maastrichtian-Danian benthic foraminifera from Site 356 were typical of lower bathyal to abyssal paleodepths, suggesting the occurrence of well-oxygenated bottom water conditions, probably under an oligotrophic regime. Increased Hg concentrations, and also Hg/TOC and $Hg/CaCO_3$ ratios, during the Maastrrichtian-Danian at Site 356 were likely connected to pulses of the Deccan Traps volcanism. When Hg concentrations and ratios were low (~65.57–65.72 Ma; P1a biozone), benthic foraminiferal species richness, heterogeneity (Shannon-Wiener), diversity (Fisher-α) and equitability slightly increased. However, additional high-resolution studies with well-constrained chronologies are needed to test this hypothesis, since several factors associated

with the K-Pg environmental perturbation, such as food availability, may have affected deep-ocean benthic foraminiferal assemblages.

Authorship statement

Guilherme Krahl: Conceptualization; Data curation; Writing – review & editing; Writing – original draft; Karlos Guilherme Diemmer Kochhann: Conceptualization; Data curation; Writing – review & editing; Gerson Fauth: Data curation; Conceptualization; Writing – review; Funding acquisition; Alcides N. Sial: Data curation; Conceptualization; Writing – review; Funding acquisition; Luiz Drude de Lacerda: Conceptualization; Writing – review; Funding acquisition.

Declaration of competing interest

The authors declare that they have no known competing financial interests or personal relationships that could have appeared to influence the work reported in this paper.

Acknowledgements

We are grateful to the International Ocean Discovery Program (IODP) for providing access to the studied samples, as well as to the support of technicians at LABOMAR (UFC), NEG- LABISE (UFPE) and itt Oceaneon (UNISINOS) during geochemical analyses. We thank E. Thomas and an anonymous reviewers for comments that helped us to significantly improve the manuscript. This research is part of the Project IODP/Capes #88887.091703/2014-1. G. Fauth acknowledges grants from CNPq (308087/2019-4). A.N.Sial acknowledges grants from FACEPE (APQ 1073-1.07/15) and CNPq (407171/2018-5). This is the NEG-LABISE contribution n. 294. G. Krahl are CAPES fellow.

Appendix A. List of identified taxa

Taxonimic list of all benthic foraminifera recognized in DSDP Site 356, arranged in a systematic order.

Allomorphina conica
Anomalinoides sp.
Anomalinoides sp. 1
Aragonia velascoensis
Astacolus sp.
Bolivinoides decorates
Bolivinoides sp.
Bolivinopsis cubensis
Bulimina aff. *kugleri*
Bulimina midwayensis
Bulimina simplex
Bulimina trinitatensis
Buliminella beaumonti
Chrysalogonium equisetiformis
Cibicidoides ? sp.
Cibicidoides hyphalus
Coryphostoma incrassate
Coryphostoma sp.
Ellipsoglandulina sp.
Fissurina spp.
Gaudryina pyramidata
Glomospira sp.
Gyroidinoides soldanii
Hauerinidae spp.
Hemirobulimina sp. 1
Laevidentalina sp. 1
Laevidentalina sp. 2
Laevidentalina sp. 3
Lagena spp.
Lagena sulcata
Lenticulina convergens
Lenticulina sp.
Marssonella sp.
Marssonella sp. 1
Nodosaria sp. 1
Nuttallides truempyi
Oridorsalis umbonatus
Paralabamina hillebrandti
Paralabamina lunata
Planulina sp.
Pleurostomella acuta
Praebulimina reussi
Pullenia bulloides
Pullenia jarvisi
Pyramidina rudita
Pyrulina spp.
Quadrimorphina allomorphinoides
Saracenaria sp.
Stensioeina beccariiformis
Stilostomella sp. 2
Strictocostella hispidula
Vulvulina spinosas

References

Arenillas, I., Arz, J.A., Gilabert, V., 2018. Blooms of aberrant planktic foraminifera across the K-Pg boundary in the Western Tethys: causes and evolutionary implications. Paleobiology 1–17.
Alegret, L., Thomas, E., 2001. Upper Cretaceous and lower Paleo-gene benthic foraminifera from northeastern Mexico. Micropaleontology 47, 269–316.
Alegret, L., Thomas, E., 2004. Benthic foraminifera and environmental turnover across the cretaceous/paleogene boundary at blake nose (ODP Hole 1049C, northwestern atlantic). Palaeogeogr. Palaeoclimatol. Palaeoecol. 208, 59–83.
Alegret, L., Thomas, E., 2007. deep-sea environments across the cretaceous/paleogene boundary in the eastern South Atlantic Ocean (ODP leg 208, Walvis Ridge). Mar. Micropaleontol. 64, 1–17.
Alegret, L., Thomas, E., Lohmann, K.C., 2012. End-Cretaceous marine mass extinction not caused by productivity collapse. Proc. Natl. Acad. Sci. Unit. States Am. 109 (3), 728–732.
Alegret, L., Thomas, E., 2013. Benthic foraminifera across the cretaceous/paleogene boundary in the southern ocean (ODP site 690): diversity, food and carbonate saturation. Mar. Micropaleontol. 105, 40–51.
Alegret, L., Molina, E., Thomas, E., 2001. Benthic foraminifera at the Cretaceous/Tertiary boundary around the Gulf of Mexico. Geology 29, 891–894.
Alegret, L., Molina, E., Thomas, E., 2003. Benthic foraminiferal turnover across the Cretaceous/Paleogene boundary at Agost (southeastern Spain): paleoenvironmental inferences. Mar. Micropaleontol. 48, 251–279.
Alvarez, L.W., Alvarez, W., Asaro, F., Michel, H.V., 1980. Extraterrestrial cause for the cretaceous–tertiary extinction. Science 208, 1095–1108.
Berggren, W.A., Aubert, J., 1975. Paleocene benthonic foraminiferal biostratigraphy, paleobiogeography and paleoecology of Atlantic–Tethyan regions: midway-type fauna. Palaeogeogr. Palaeoclimatol. Palaeoecol. 18, 73–192.
Berggren, W.A., Miller, K.G., 1989. Cenozoic bathyal and abyssal calcareous benthic foraminiferal zonation. Micropaleontology 35, 308–320.
Boersma, A., 1977. Cenozoic planktonic foraminifera - DSDP leg 39 (South Atlantic). Initial Rep. Deep Sea Drill. Proj. 39, 567–592.
Boltovskoy, E., Boltovskoy, D., 1989. Paleocene-pleistocene benthic foraminiferal evience of major paleoceanographic events in the eastern South atlantic (DSDP site 525, Walvis Ridge). Mar. Micropaleontol. 14, 283–316.
Boltovskoy, E., Watanabe, S., 1994. Biostratigraphy of tertiary and quaternary benthic bathyal foraminifers of DSDP site 317 (tropical pacific). Mar. Micropaleontol. 23, 101–120.
Bralower, T.J., Cosmidis, J., Heaney, P., Kump, L.R., Morgan, J., Harper, D., Lyons, S.L., Freeman, K.H., Grice, K., Wendler, J., Zachos, J.C., Artemieva, N., Gulick, S., House, C., Jones, H.L., Lowery, C.L., Nims, C., Schaefer, B., Si, A., Thomas, E., Vajda, V., 2020. Origin of a global carbonate layer deposited in the aftermath of the Cretaceous-Paleogene boundary impact. Earth Planet Sci. Lett. 548, 1–17.
Caruso, A., Cosentino, C., Tranchina, L., Brai, M., 2011. Response of benthic foraminifera to heavy metal contamination in marine sediments (Sicilian coasts, Mediterranean Sea). Chem. Ecol. 27, 9–30.
Charbonnier, G., Adatte, T., Föllmi, K.B., Suan, G., 2020. Effect of intense weathering and post-depositional degradation of organic matter on Hg/TOC proxy in organic-rich sediments and its implications for deep-time investigations. G-cubed 21. https://doi.org/10.1029/2019GC08707.
Coccioni, R., Savelli, D., 1983. Osservazioni stratigra'che sullimite K-T della sezione di Coldorse (Sella S. Abbondio,Appennino umbro-marchigrino). Acta Nat. l'Ateneo Parm. 19, 199–212.

Courtillot, V., Renne, P.R., 2003. On the ages of flood basalt events Sur l'âge des trapps basaltiques. Compt. Rendus Geosci. 335 (1), 113–140.
Culver, S.J., 1988. New foraminiferal depth zonation of the north- western Gulf of Mexico. Palaios 3, 69–8.
Culver, S.J., 2003. Benthic foraminifera across the Cretaceous/Tertiary (K/T) boundary: a review. Mar. Micropaleontol. 47, 177–226.
Dinarès-Turell, J., Westerhold, T., Pujalte, V., Röhl, U., Kroon, D., 2014. Astronomical calibration of the danian stage (early Paleocene) revisited: settling chronologies of sedimentary records across the atlantic and pacific oceans. Earth Planet Sci. Lett. 405, 119–131.
D'Hondt, S., 2005. Consequences of the cretaceous/paleogene mass extinction for marine ecosystems. Annu. Rev. Ecol. Evol. Syst. 36, 295–317.
Driscoll, C.T., Mason, R.P., Chan, H.M., Jacob, D.J., Pirrone, N., 2013. Mercury as a global pollutant: sources, pathways, and effects. Environ. Sci. Technol. 47, 4967–4983.
Frontalini, F., Buosi, C., Da Pelo, S., Coccioni, R., Cherchi, A., Bucci, C., 2009. Benthic foraminifera as bio-indicators of trace element pollution in the heavily contaminated Santa Gilla lagoon (Cagliari, Italy). Mar. Pollut. Bull. 58, 858–877.
Frontalini, F., Greco, M., Di Bella, L., Lejzerowicz, F., Reo, E., Caruso, A., Cosentino, C., Maccotta, A., Scopelliti, G., Nardelli, M.P., Losada, M.T., du Châtelet, E.A., Coccioni, R., Pawlowsk, J., 2018. Assessing the effect of mercury pollution on cultured benthic foraminifera community using morphological and eDNA metabarcoding approaches. Mar. Pollut. Bull. 129, 512–524.
Font, E., Adatte, T., Sial, A.N., Drude de Lacerda, L., Keller, G., Punekar, J., 2016. Mercury anomaly, Deccan volcanism, and the end-cretaceous mass extinction. Geology 44, 171–174.
Gallala, N., Zaghbib-Turki, D., Arenillas, I., Arz, J.A., Molina, E., 2009. Catastrophic mass extinction and assemblage evolution in planktic foraminifera across the Cretaceous/Paleogene (K/Pg) boundary at Bidart (SWFrance). Marine. Micropaleontology 72, 196–209.
Gebka, K., Beldowska, M., Saniewska, D., Kuliński, K., Bełdowski, J., 2018. Watershed characteristics and climate factors effect on the temporal variability of mercury in the southern Baltic Sea rivers. J. Environ. Sci. 68, 55–64.
Gradstein, F.M., Ogg, J.G., Schmitz, M.D., Ogg, G.M., 2012. The Geological Time Scale 2012, vol. 2. Elsevier, Amsterdam, p. 1144.
Grasby, S.E., Beauchamp, B., Bond, D.P.G., Wignall, P.B., Sanei, H., 2016. Mercury anomalies associated with three extinction events (capitanian crisis, latest permian extinction and the smithian/spathian extintion) in NW pangea. Geol. Mag. 153, 285–297.
Hammer, O., Harper, D.A.T., Ria, P.D., 2001. Past: Palaeonthological Statistics Software Package for Education and Data Analysis. Version. 1.37.
Hayward, B.W., Sabaa, A.T., Kawagata, S., Grenfell, H.R., 2012. The early pliocene re-colonisation of the deep mediterranean sea by benthic foraminifera and their pulsed late pliocene–middle pleistocene decline. Mar. Micropaleontol. 71 (3–4), 97–112.
Hull, P.M., Norris, R.D., 2011. Diverse patterns of ocean export productivity change across the Cretaceous/Paleogene boundary: new insights from biogenic barium. Paleoceanography 26 (3).
Hull, P.M., Bornemann, A., Penman, D.E., Henehan, M.J., Norris, R.D., Wilson, P.A., Blum, P., Alegret, L., Batenburg, S.J., Bown, P.R., Bralower, T.J., Cournede, C., Deutsch, A., Donner, B., Friedrich, O., Jehle, S., Kim, H., Kroon, D., Lippert, P.C., Loroch, D., Moebius, I., Moriya, K., Peppe, D.J., Ravizza, G.E., Rohl, U., Schueth, J. D., Sepulveda, J., Sexton, P.F., Sibert, E.C., Sliwinska, K.K., Summons, R.E., Thomas, E., Westerhold, T., Whiteside, J.H., Yamaguchi, T., Zachos, J.C., 2020. On impact and volcanism across the Cretaceous-Paleogene boundary. Science 367, 266–272.
Jiang, G.B., Shi, J.B., Feng, X.B., 2006. Mercury pollution in China. Environ. Sci. Technol. 40, 3672–3678.
Jones, M.T., Percival, L.M.E., Stokke, E.W., Frielin, J., Mather, T.A., Riber, L., Schubert, B.A., Schultz, B., Tegner, C., Planke, S., Svensen, H.H., 2019. Mercury anomalies across the palaeocene–eocene thermal maximum. Clim. Past 15, 217–236.
Kochhann, K.G.D., Lopes, F.M., Krahl, G., Aguiar, E., Fauth, G., 2014. Late cretaceous-early paleogene (?Turonian to early danian) planktic foraminifera from DSDP site 356: a biostratigraphic reappraisal. Rev. Bras. Palaontol. 17, 157–168.
Koutsoukos, E.A.M., 1996. Phenotypic experiments into new pelagic niches in early Danian planktonic foraminifera: aftermath of the K/T boundary event. Biotic recovery from mass extinction events. Geological Society, London, Special Publications 102, 319–335.
Koutsoukos, E.A.M., 2014. Phenotypic plasticity, speciation, and phylogeny Early Danian Planktonic foraminifera. J. Foraminifer. Res. 44, 109–142.
Krahl, G., Koutsoukos, E.A.M., Fauth, G., 2017. Paleocene planktonic foraminifera from DSDP site 356, South Atlantic: paleoceanographic inferences. Mar. Micropaleontol. 135, 1–14.
Loeblich, A.R., Tappan, H., 1987. Foraminiferal Genera and Their Classification. Van Nostrand Reinhold Company, New York, p. 970.
Luterbacher, H., Premilo-Silva, I., 1962. Note préliminaire sur une révison du profil de Gubbio, Italie. Riv. Ital. Paleontol. Stratigr. 68 (2), 253–288.
Luterbacher, H., Premilo-Silva, I., 1964. Biostratigrafia del limite Cretaceo-Terziario nell'Appennino Centrale. Rivista Italiana di Paleontologia 70, 67–128.
Molina, E., 2015. Evidence and causes of the main extinction events in the Paleogene based on extinction and survival patterns of foraminifera. Earth Sci. Rev. 140, 166–181.
Perch-Nielsen, K., Supko, P.R., Boersma, A., Carlson, R.L., Dinkelman, M.G., Fodor, R.V., Kumar, N., McCoy, F., Thiede, J., Zimmerman, H.B., 1977. Site 356: São Paulo Plateau. In: Supko, P.R. (Ed.), Deep Sea Drilling Program Initial Reports, vol. 39. United States Government Printing Office, Washington, pp. 41–230.
Percival, L.M.E., Witt, M.L.I., Mather, T.A., Hermoso, M., Jenkyns, H.C., Hesselbo, S.P., Al-Suwaidi, A.H., Storm, M.S., Xu, W., Ruhl, M., 2015. Globally enhanced mercury deposition during the end-pliensbachian extinction and toarcian oae: a link to the karoo–ferrar large igneous province. Earth Planet Sci. Lett. 428, 267–280.
Smit, J., 1990. Meteorite impact, extinctions and the Cretaceous–Tertiary boundary. Geol. Mijnbouw 69, 187–204.
Schulte, P., Alegret, L., Arenillas, I., Arz, J.A., Barton, P.J., Bown, P.R., Bralower, T.J., Christeson, G.L., Claeys, P., Cockell, C.S., Collins, G.S., Deutsch, A., Goldin, T.J., Goto, K., Grajales-Nishimura, J.M., Grieve, R.A.F., Gulick, S.P.S., Johnson, K.R., Kiessling, W., Koeberl, C., Kring, D.A., MacLeod, K.G., Matsui, T., Melosh, J., Montanari, A., Morgan, J.V., Neal, C.R., Nichols, D.J., Norris, R.D., Pierazzo, E., Ravizza, G., Rebolledo-Vieyra, M., Reimold, W.U., Robin, E., Salge, T., Speijer, R.P., Sweet, A.R., Urrutia-Fucugauchi, J., Vajda, V., Whalen, M.T., Willumsen, P.S., 2010. The Chicxulub asteroid impact and mass extinction at the Cretaceous–Paleogene boundary. Science 327, 1214–1218.
Schoene, B., Eddy, M.P., Samperton, K.M., Keller, C.B., Keller, G., Adatte, T., Khadri, S.F. R., 2019. U-Pb constraints on pulsed eruption of the Deccan Traps across the end-Cretaceous mass extinction. Science 363 (6429), 862–866.
Schoene, B., Eddy, M.P., Keller, C.B., Samperton, K.M., 2021. An evaluation of deccan traps eruption rates using geochronologic data. Geochronology 3, 181–198.
Schönfeld, J., Burnett, J., 1991. Biostratigraphical correlation of the Campanian-Maastrichtian boundary: Läger-dorf-Henmoor (northwestern Germany); DSDP Sites 548A, 549 and 551 (eastern North Atlantic) with palaeo-biogeographical and palaeoceanographical implications. Geol. Mag. 128, 479–503.
Self, S., Blake, S., Sharma, K., Widdowson, M., Sephton, S., 2008. Sulfur and chlo-rine in Late Cretaceous Deccan magmas and eruptive gas release. Science 319, 1654–1657.
Sepúlveda, J., Alegret, L., Thomas, E., Haddad, E., Cao, C., Summous, R.E., 2012. Stable isotope constraints on marine productivity across the cretaceous-paleogene mass extinction. Paleoceanography and Paleoclimatology 34 (7), 2018PA003442.
Sial, A.N., Chen, J.B., Lacerda, L.D., Peralta, S., Gaucher, C., Frei, R., Cirilli, S., Ferreira, V.P., Marquillas, R.A., Barbosa, J.A., Pereira, N.S., Belmino, I.K.C., 2014. High-resolution Hg Chemostratigraphy: a contribution to the distinction of chemical fingerprints of the Deccan volcanism and Cretaceous-Paleogene boundary impact event. Palaeogeogr. Palaeoclimatol. Palaeoecol. 414, 98–115.
Sial, A.N., Chen, J., Lacerda, L.D., Frei, R., Tewari, V.C., Pandit, M.K., Gaucher, C., Ferreira, V.P., Cirilli, S., Peralta, S., Korte, C., Barbosa, J.A., Pereira, N.S., 2016. Mercury enrichment and Hg isotopes in Cretaceous–Paleogene boundary successions: links to volcanism and palaeoenvironmental impacts. Cretac. Res. 66, 60–81.
Sial, A.N., Chen, J., Lacerda, L.D., Frei, R., Higgins, J.A., Tewari, V.C., Gaucher, C., Ferreira, V.P., Cirilli, S., Kort, C., Barbosa, J.A., Pereira, N.S., Ramos, D.S., 2018. Chemostratigraphy across the cretaceous-paleogene (K-pg) boundary: testing the impact and volcanism hypotheses. In: Sial, A.N., Gaucher, C., Muthuvairavasemy, R., Ferreira, V.P. (Eds.), Chenostratigraphy across Major Chronological Boundaries, Geophysical Monograph 240. Wiley, 293–260.
Sizmur, T., O'Driscoll, N., Cai, Y., 2018. JES special issue in mercury biogeochemistry and fate. J. Environ. Sci. 68, 1–4.
Speijer, R.P., 1994. Extinction and Recovery Patterns in Benthic Foraminiferal Paleocommunities across the Cretaceous/Paleogene and Paleocene/Eocene Boundaries, vol. 124. Geologica Ultraiectina - Mededelingen van de Faculteit Aardwetenschappen Universiteit Utrecht, pp. 1–191.
Sprain, C.J., Renne, P.R., Vanderklusen, L., Pande, K., Self, S., Mittal, T., 2019. The eruptive tempo of Deccan volcanism in relation to the Cretaceous-Paleogene boundary. Science 363 (6429), 866–870.
Stax, R., Stein, R., 1995. Data report: organic carbon and carbonate records from Detroit seamount and Patton-Murray seamount: results from sites 882 and 887 (north Pacific Transect). Proc. Ocean Drill. Progr. Sci. Results 145, 645–655.
Thomas, E., 1990. Late cretaceous-early eocene masse extinctionsin the deep-sea in global catastrophes. In: Sharpton, V.L., Ward, P.D. (Eds.), Global Catastrophes, vol. 247. Spec. Pap. Geol. Soc. Am., pp. 481–496
Tjalsma, R.C., Lohmann, G.P., 1983. Paleocene-Eocene Bathyal and Abyssal Benthic Foraminífera from the Atlantic Ocean, vol. 4. Micropaleontology Special Publication, p. 90.
Van Morkhoven, F.P.C.M., Berggren, W.A., Edwards, A.S., 1986. Cenozoic cosmopolitan deep-water benthic foraminifera. Bull. Cent. Rech. Explor.-Prod. Elf-Aquitaine - Mem. 11, 421.
Varekamp, J.C., Buseck, P.R., 1981. Mercury emissions from mount st helens during september 1980. Nature 293, 555–556.
Varekamp, J.C., Buseck, P.R., 1986. Global mercury flux from volcanic and geothermal sources. Appl. Geochem. 1 (1), 65–73.
Widmark, J.G.V., 2000. Biogeography of terminal Cretaceous benthic foraminifera: deep-water circulation and trophic gradients in the deep South Atlantic. Cretac. Res. 21, 367–379.
Widmark, J.G.V., Speijer, R.P., 1997. Benthic foraminiferal eco-marker species of the terminal Cretaceous (late Maastrichtian) deep-sea Tethys. Mar. Micropaleontol. 31, 135–155.
Widmark, J.G.V., Malmgren, B., 1992. Benthic foraminiferalchanges across the Cretaceous-Tertiary boundary in thedeep sea; DSDP Sites 525, 527, and 465. J. Foraminifer. Res. 22, 81–113.
Zachos, J.C., Arthur, M.A., 1986. Paleoceanography of the cretaceous/tertiary boundary event: inferences from stable isotopic and other data. Paleoceanography 22, 5–26.